Localization of MreB in *Rhodobacter sphaeroides* under Conditions Causing Changes in Cell Shape and Membrane Structure†

Peter M. Slovak, George H. Wadhams, and Judith P. Armitage*

Department of Biochemistry, University of Oxford, Oxford, United Kingdom

MreB is thought to be a bacterial actin homolog that defines the morphology of rod-shaped bacteria. *Rhodobacter sphaeroides* changes shape, from a rod to coccobacillus, and undergoes extensive cytoplasmic membrane invagination when it switches from aerobic to photoheterotrophic growth. The role of MreB in defining *R. sphaeroides* shape was therefore investigated. Attempts at deleting or insertionally inactivating *mreB* were unsuccessful under all growth conditions. Immunofluorescence microscopy showed MreB localized to mid-cell in elongating cells under both aerobic and photoheterotrophic conditions. Three-dimensional reconstruction showed that MreB formed a ring at mid-cell. MreB remained at mid-cell as septation began but localized to new sites in the daughter cells before the completion of septation. MreB localized to putative septation sites in cephalexin-treated filamentous cells. Genomic single-copy *mreB* was replaced with *gfp-mreB*, and green fluorescent protein (GFP)-MreB localized in the same pattern, as seen with immunofluorescence microscopy. Some of the cells expressing GFP-MreB were abnormal, principally displaying an increase in cell width, suggesting that the fusion was not fully functional in all cells. GFP-MreB localized to swellings at mid-cell in cells treated with the penicillin-binding protein 2 inhibitor amdinocillin. These data suggest that MreB is essential in *R. sphaeroides*, performing a role at mid-cell in elongating cells, and in early septation, putatively in the cytoplasmic control of the peptidoglycan synthetic complexes.

MreB, encoded by *mreB* of the *mre* locus, is thought to be a bacterial actin homolog. The *mre* locus in *Escherichia coli* and *Bacillus subtilis* also includes *mreC* and *mreD* (13, 28). In the gram-negative rod-shaped *E. coli*, deletion of *mreB* or of the *mre* locus results in spherical-shaped cells (12, 29). In the gram-positive rod-shaped *B. subtilis*, MreB appears to be essential, as depletion of the protein produces rounded cell shapes and these morphologically abnormal cells eventually lyse (11). MreB, in both *E. coli* and *B. subtilis*, has been shown to localize just below the cytoplasmic membrane in a helical configuration (11, 20). In *E. coli* MreB localizes both as a helix that spans the longitudinal axis of the cell and as a transverse band at mid-cell. In *B. subtilis* MreB localizes mainly as a transverse helical band at mid-cell. These studies suggest that MreB forms a filamentous subcellular helix that defines rod-shaped cell morphology. The MreB crystal structure confirmed the structural predictions that it belongs to the actin family of proteins (26). The structural relationship was extended by demonstrating nucleotide-dependent MreB polymerization with the MreB monomers displaying a spacing of 51 Å within the filament reminiscent of the 55-Å longitudinal spacing of actin monomers within actin filaments (26). Control of eukaryotic cell shape involves actin, and thus the functional and structural similarity between MreB and actin led to the proposal that MreB is a bacterial actin homolog.

In bacteria, the peptidoglycan layer principally determines cell shape. Peptidoglycan consists of glycan strands cross-linked by peptide side chains. The peptidoglycan subunits, disaccharide peptides, are assembled in the cytoplasm and linked to the preexisting peptidoglycan layer in the periplasm by transglycosylase and transpeptidation reactions. In *E. coli* two distinct phases of peptidoglycan synthesis occur. In cells undergoing septation the transpeptidase FtsI, in concert with the integral membrane protein FtsW, mediates the insertion of peptidoglycan that forms the new poles of the daughter cells (6). In elongating cells the transpeptidase penicillin-binding protein 2 (PBP2) and RodA function in the peptidoglycan-driven extension of the longitudinal axis (3).

Cell shape mutants typically possess mutations in genetic loci that encode proteins involved in peptidoglycan synthesis. The effects of *mreB* deletion in *E. coli* and MreB depletion in *B. subtilis* suggest a role for MreB in peptidoglycan synthesis (11, 12). However, these studies have also been used to suggest that MreB may define rod-shaped morphology, possibly by forming a structural brace (5), while additional studies suggest that MreB may function in chromosome segregation (12, 24). Thus, the role performed by MreB is at present uncertain and may vary between species.

Rhodobacter sphaeroides is an α-subgroup, purple nonsulfur photosynthetic bacterium which displays different cellular morphologies under different growth conditions (2). Aerobically grown cells are rod shaped, while photoheterotrophically grown cells are coccobacillus shaped. The extent of the coccobacillus morphology is dependent on the available light, with low light levels producing a more pronounced spherical shape. Associated with the various cell shapes is an alteration in the structure of the cytoplasmic membrane. In aerobically grown cells the cytoplasmic membrane is smooth, whereas in photoheterotrophically grown cells the cytoplasmic membrane invaginates, forming the support for the photosynthetic appa-

* Corresponding author. Mailing address: Department of Biochemistry, University of Oxford, South Parks Rd., Oxford, OX1 3QU United Kingdom. Phone: (44) 186 527 5299. Fax: (44) 186 527 5297. E-mail: armitage@bioch.ox.ac.uk.

TABLE 1. Bacterial strains and plasmids used in this study

Strain or plasmid	Characteristics	Source or reference
E. coli strains		
DH5α	General cloning strain, allows blue-white screening during cloning	Gibco-BRL
S17-1λ*pir*	Strain capable of mobilizing the suicide vector pK18*mobsacB* into *R. sphaeroides*, Sm^r	15
M15	Protein expression host	Qiagen
R. sphaeroides strains		
WS8N	Spontaneous nalidixic acid-resistant mutant of wild-type WS8	23
JPA187	WS8N containing a *gfp-mreB* fusion in place of the genomic *mreB*	This study
Plasmids		
pUC19	High-copy-number cloning vector, Ap^r	Pharmacia
pK18*mobsacB*	Allelic exchange suicide vector, Km^r	19
pHP45Ω	Carries the omega cartridge, Sm^r	17
pEGFP-N1	GFP fusion vector, Km^r	Clontech
pQE80	P$_{tac}$-based expression vector; introduces RGS(H)$_6$ sequence at the N termini of expressed proteins; Ap^r	Qiagen
pREP4	Plasmid carrying the lacI gene; compatible with pQE80; reduces leaky expression from the *tac* promoter of pQE80; Km^r	Qiagen
c125	pLA2917 containing ca. 25 kb of *R. sphaeroides* DNA, Tc^r	22
pPKS1	Derivative of pK18*mobsacB* containing the region upstream of *mreB*	This study
pPKS2	Derivative of pK18*mobsacB* containing the regions upstream and downstream of *mreB*	This study
pPKS2Ω	Derivative of pPKS2 containing the omega cartridge from pHP45Ω between the regions upstream and downstream of *mreB*	This study
pBS1	Derivative of pK18*mobsacB* containing the region upstream of *mreB* and *gfp*	This study
pBS2	Derivative of pK18*mobsacB* containing the *gfp-mreB* fusion; the region upstream of *mreB* and *gfp* and the upstream region of *mreB*	This study
pMLP1	Derivative of pQE80 containing *mreB*	This study

ratus. The extent of the invagination is dependent on the available light, with low light levels producing a very extensively invaginated cytoplasmic membrane.

The aims of this study were to determine the cellular requirement for MreB and its role in rod- and coccobacillus-shaped *R. sphaeroides* cells.

MATERIALS AND METHODS

Strains and growth conditions. Bacterial strains and plasmids are listed in Table 1. *R. sphaeroides* strains were cultured in succinate medium (21) at 30°C either aerobically in the dark with shaking or photoheterotrophically with either 1 or 35 μmol m^{-2} s^{-1} of light. *E. coli* DH5α was used for all molecular cloning, strain S17-1 λ*pir* was used for conjugal transfer into *R. sphaeroides*, and strain M15 pREP4 was used for protein expression. *E. coli* strains were cultured in Luria-Bertani medium at 37°C with shaking. Antibiotics were used at 25 μg ml^{-1} for kanamycin, nalidixic acid, and streptomycin and at 100 μg ml^{-1} for ampicillin.

For inhibition studies, early-log-phase *R. sphaeroides* cells were cultured aerobically either in the presence of amdinocillin at 25 μg ml^{-1} for 1 h at 30°C or in the presence of cephalexin at 2.5 μg ml^{-1} for 4 h at 30°C.

Molecular genetic techniques. All cloning steps were performed as described by Sambrook and Russell (18). Sequencing-quality DNA was prepared using the WizardPlus kit (Promega), sequenced by the University of Oxford Biochemistry sequencing service, and analyzed with the GCG software package (University of Wisconsin). All primers were supplied by Genosys Biotechnologies Inc.

Cell scoring. Images were acquired of wild-type cells grown aerobically or photoheterotrophically, at different light intensities, by differential interference contrast (DIC) microscopy using a Nikon TE200 microscope with a cooled charge-coupled device (CCD) camera (Hamamatsu). Cells were scored as newly divided (septation clearly just completed), elongating (length extension occurring, no septum invagination visible), septation initiated (length extended, septum invagination beginning), or septation nearing completion (septum deeply invaginated, daughter cells clearly forming). Following classification the cell lengths and cell widths were measured using SimplePCI image analysis software (Digital Pixel). A total of ≥25 cells were analyzed, from ≥5 fields of view, for each cell cycle stage. The images were processed with SimplePCI image analysis software (Digital Pixel).

For scoring green fluorescent protein (GFP)-MreB-expressing cells, images

were acquired as outlined above. For wild-type populations the scoring system was identical to that described above. For GFP-MreB-expressing populations, cells were scored as normal (cell length and cell width similar or identical to wild-type cells), mildly abnormal (cell length and/or cell width varying in comparison to wild type), or severely abnormal (cell length and/or cell width varying extensively in comparison to wild type). The normal, mildly abnormal, or severely abnormal cells were grouped separately into the outlined cell cycle stage classifications. Following classification the cell lengths and cell widths were measured using SimplePCI image analysis software (Digital Pixel). For the wild-type cells, a total of ≥25 cells were analyzed, from ≥5 fields of view, for each cell cycle stage. For GFP-MreB-expressing populations a total of ≥25 normal, mildly abnormal, or severely abnormal cells were analyzed, from ≥10 fields of view, for each cell cycle stage. The images were processed with SimplePCI image analysis software (Digital Pixel).

Protein expression construct. *mreB* was amplified by PCR using primers that omitted the start codon and included 5′ BamHI and 3′ HindIII sites. The PCR product was ligated into pQE80 (QIAGEN) to produce pMLP1. The construct was sequenced to ensure the coding sequence contained no errors.

Protein purification and antibody production. His-tagged MreB was expressed in *E. coli* M15 pREP4 cells containing pMLP1. Purification was performed as described previously (14). A rabbit antibody was raised against purified MreB (Eurogentec).

Cell fractionation. Cell fractionation was performed as described previously (31) with the following modifications. A 100-ml culture of aerobically grown *R. sphaeroides* at an optical density at 700 nm of 0.6 was harvested by centrifugation. The cells were spheroplasted by resuspension in 1 ml of 0.15 M Tris-HCl (pH 8.0) containing 0.5 M sucrose, 1 mg of lysozyme, and 10 mM EDTA. The spheroplasts were harvested by centrifugation, gently lysed by the addition of 5 ml of water, and kept on ice for 3 h with gentle mixing every 30 min. Centrifugation at 25,000 × g for 30 min removed cell debris, and centrifugation at 100,000 × g for 120 min pelleted the cell membranes. The cytoplasmic fraction was decanted and stored. The cell membrane pellet was resuspended in water, in a volume equivalent to that of the cytoplasmic fraction, and stored.

Immunoblotting. Samples of membrane and cytoplasmic fractions were mixed with an equal volume of 2× sodium dodecyl sulfate-polyacrylamide gel electrophoresis loading buffer. Samples were run on a 12% polyacrylamide gel and transferred to polyvinylidene difluoride membranes (Bio-Rad) by electroblotting. The polyvinylidene difluoride membranes were blocked overnight at room temperature. MreB antibodies were added at a 1:2,000 dilution in blocking solution and incubated at room temperature for 1 h. Anti-rabbit–horseradish

TABLE 2. Cell shape properties of *R. sphaeroides* grown under different growth conditions[a]

Growth condition	Mean (SEM) at cell cycle stage							
	Newly formed		Elongating		Septation initiated		Septation nearing completion	
	Length	Width	Length	Width	Length	Width	Length	Width
Aerobic	1.73 (0.02)	1.17 (0.01)	2.21 (0.03)	1.16 (0.01)	2.67 (0.03)	1.13 (0.01)	3.01 (0.03)	1.16 (0.01)
High light	1.52 (0.02)	1.18 (0.01)	1.99 (0.04)	1.19 (0.01)	2.37 (0.02)	1.17 (0.01)	2.66 (0.02)	1.16 (0.01)
Low light	1.40 (0.01)	1.14 (0.01)	1.79 (0.02)	1.20 (0.01)	2.15 (0.02)	1.14 (0.01)	2.45 (0.03)	1.14 (0.02)

[a] Cells were grown aerobically or photoheterotrophically with different light levels. Cell lengths and cell widths (in micrometers) were measured from a total of ≥25 cells, from ≥5 fields of view, for each cell cycle stage. Mean and standard error values are shown.

peroxidase conjugate (DAKO) was added at a 1:1,000 dilution in blocking solution, and the membrane was incubated as above. Membranes were washed with phosphate-buffered saline (PBS) and 0.1% (vol/vol) Tween. An enhanced chemiluminescence kit (Amersham) was used for detection.

Deletion constructs. An *mreB* in-frame deletion construct was generated by amplifying, by PCR, a 0.5-kb region immediately upstream of *mreB* with primers that encompassed the start codon and included 5′ EcoRI and 3′ BamHI sites. A 0.5-kb region that included the seven 3′ codons and the downstream flanking DNA of *mreB* was amplified by PCR using primers that included 5′ BamHI and 3′ HindIII sites. The first PCR product was ligated into pK18*mobsacB* to produce pPKS1. The second PCR product was ligated into pPKS1 to generate the final construct, pPKS2. An *mreB* insertional inactivation construct was generated by excising the omega cartridge from pHP45Ω with BamHI and cloning this fragment into BamHI-cut pPKS2 to produce pPKS2Ω. Constructs were sequenced to ensure that upstream and downstream regions are in frame and contained no errors. The constructs were introduced into *R. sphaeroides* by allelic exchange as described previously (8, 19).

Fixation and permeabilization. Cells were fixed and permeabilized as described previously (9) with the following modifications. A 0.5-ml volume of bacterial culture was mixed with an equal volume of concentrated fixative solution. Cells cultured in succinate medium were fixed with a final concentration of 1.3% (vol/vol) paraformaldehyde and 0.02% (vol/vol) glutaraldehyde in PBS (pH 7.4) for 15 min at room temperature and for 30 min on ice. The fixed bacteria were washed three times in PBS at room temperature and then resuspended in 200 μl of glucose-Tris-EDTA. A freshly prepared lysozyme solution, in PBS, was added to a final concentration of 2 mg ml^{-1}. Samples (25 μl) were immediately distributed onto wells of a multiwell microscope slide (Hendley-Essex) which had been treated with 0.01% (wt/vol) poly-L-lysine (Sigma). After 2 min the liquid was aspirated from the wells, which were then allowed to dry for 4 min. A 25-μl volume of PBS was added to each well for 1 min and then removed by aspiration. A 25-μl volume of blocking solution (5% bovine serum albumin in PBS) was added to each well, and the slides were incubated for 30 min at room temperature.

Immunofluorescence staining. Immunofluorescence staining was performed as described previously (9) with the following modifications. Cells were incubated with a 1:10,000 dilution in blocking solution of rabbit polyclonal anti-MreB antibodies overnight at 4°C. The wells were washed 20 times with blocking solution. Cells were then incubated with a 3:1,000 dilution in blocking solution of fluorescein isothiocyanate–anti-rabbit antibodies (Sigma) for 3 h at room temperature in the dark. The cells were washed 10 times with blocking solution and 10 times with PBS. Slides were mounted with 2 μl of Vectashield antifade (Vector Laboratories).

Construction of a *gfp-mreB* fusion strain. A 0.5-kb region immediately upstream of *mreB* was amplified by PCR using primers that omitted the start codon and included a 5′ EcoRI site and a 3′ sequence complementary to the beginning of *egfp*. The 0.8-kb *egfp* was amplified by PCR using primers that omitted the stop codon and included a 5′ sequence complementary to the 15-bp region immediately upstream of *mreB* and a 3′ XbaI site. These PCR products were used as templates for further PCR, using the 5′ primer from the *mreB* upstream PCR and the 3′ primer from the *egfp* PCR, to generate a 1.3-kb fragment. The PCR product, upstream *mreB* fused to *egfp*, was ligated into pK18*mobsacB* to produce pBS1. A 0.5-kb region immediately downstream of the *mreB* start codon was amplified by PCR using primers that included 5′ XbaI and 3′ HindIII sites. This PCR product was ligated into pBS1 to generate the final construct pBS2. The construct was sequenced to ensure that upstream and downstream regions were in frame and contained no errors. The construct was inserted into *R. sphaeroides* by allelic exchange as described previously (8, 19).

Fluorescence analysis. For immunofluorescence microscopy, DIC and fluorescence images were acquired using a Nikon TE200 microscope with a GFP filter set and recorded with a cooled CCD camera (Hamamatsu). Z-series were captured with a custom-built Piezo driven (Physik Instruments) mechanical stage. The images were processed with SimplePCI image analysis software (Digital Pixel).

For GFP-MreB localization in log phase, cultures were embedded in 1.2% agarose on microscope slides. Phase-contrast and fluorescence images were acquired using a Zeiss Axiovert 135TV microscope with a fluorescein isothiocyanate filter set and recorded with a cooled CCD camera (Digital Pixel Advanced Imaging Systems). The images were processed with image analysis software (METAMORPH 6.1).

For GFP-MreB localization through the cell cycle, log-phase cultures were embedded in 0.8% succinate agarose on microscope slides. DIC and fluorescence images were acquired as described for immunofluorescence microscopy at 20-min intervals. The images were processed with SimplePCI image analysis software (Digital Pixel).

RESULTS

***R. sphaeroides* cell shape changes under different growth conditions.** The cell shape properties of *R. sphaeroides* grown aerobically or photoheterotrophically with different light levels were determined. Cells were scored as newly formed (septation clearly just completed), elongating (length extension occurring, no septum invagination visible), septation initiated (length extended, septum invagination beginning), or septation nearing completion (septum deeply invaginated, daughter cells clearly forming). Following cell stage classification, the cell lengths and cell widths were measured.

The cell width remained fairly constant (1.14 to 1.20 μm), while the cell length changed significantly under different growth conditions (Table 2). The longest cell lengths were observed in aerobic cells. The shortest cell lengths were seen in photoheterotrophic cells grown under low light intensities, with intermediate cell lengths observed in photoheterotrophic cells grown under much higher light intensities. These data demonstrate that the previously observed differences in *R. sphaeroides* morphologies grown under different conditions (2) result from an alteration in cell length rather than a modification of the cell width.

Identification of the *mre* and *mrd* loci in *R. sphaeroides* strain WS8N. Genome sequencing of the closely related *R. sphaeroides* strain 2.4.1 indicated the presence of an *mre-mrd* locus encoding putative cell shape-determining proteins (http://genome.jgi-psf.org/draft_microbes/rhosp/rhosp.home.html). *mreB* and *rodA* were amplified by PCR from *R. sphaeroides* WS8N genomic DNA and used to probe a cosmid library of this strain (22). Cosmid c125 was found to contain both the *mre* and *mrd* loci, and the DNA sequence of this region was determined (EMBL database accession no. AJ605582). DNA sequence and open reading frame prediction software (Clone Manager 7) identified five putative genes in this region (Fig. 1).
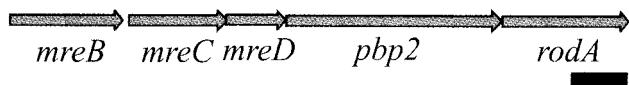
FIG. 1. *mre* and *mrd* loci of *R. sphaeroides* WS8N. *mreB*, *mreC*, and *mreD* form the *mre* locus; *pbp2* and *rodA* form the *mrd* locus. These two loci may form a single operon. Bar, 500 bp.

The *mreB*, *mreC*, and *mreD* genes, forming the *mre* gene cluster, were located adjacent to the *pbp2* and *rodA* genes, which form the *mrd* gene cluster. These genes are all orientated in the same direction and the *mreD* stop codon overlaps the *pbp2* start codon, suggesting that the *mre* and *mrd* loci form an operon in *R. sphaeroides*.

Sequence analysis of the Mre and Mrd proteins. The 345-amino-acid sequence of *R. sphaeroides* MreB shares 58 and 53% identity with the *E. coli* and *B. subtilis* proteins, respectively. The high level of sequence homology for *R. sphaeroides* MreB is consistent with that previously observed for the protein between other bacterial species (1, 27). Hydropathy profiles (TMHMM [http://www.cbs.dtu.dk/services/TMHMM/]) and TMPred (10) predicted that the 37-kDa *R. sphaeroides* MreB was a soluble, cytoplasmic protein.

R. sphaeroides MreC, MreD, PBP2, and RodA share 27, 13, 36, and 45% identity with the *E. coli* proteins, respectively, and 28, 11, 23, and 28% identity with the *B. subtilis* proteins, respectively. Hydropathy profiles (TMHMM and TMPred) predicted the presence of one N-terminal transmembrane α-helix in both MreC and PBP2 and multiple transmembrane α-helices in both MreD and RodA. The levels of identity and predicted membrane topologies of the *R. sphaeroides* proteins are similar to those previously observed between the bacterial paradigms and other bacterial species (1).

MreB is a cytoplasmic protein. The cellular localization of MreB was determined by cell fractionation and Western blotting. MreB localizes just below the cytoplasmic membrane in *E. coli* and *B. subtilis* (11, 20). MreB may either associate with the cytoplasmic membrane through inherent properties of the protein or localization may depend upon additional proteins. *R. sphaeroides* spheroplasts were gently lysed, and the membrane and cytoplasmic fractions were subjected to Western blotting.

R. sphaeroides MreB localized to the cytoplasmic fraction (data not shown), confirming the in silico prediction of MreB as a soluble, cytoplasmic protein. This suggests MreB is only weakly associated with the cytoplasmic membrane.

MreB appears essential for *R. sphaeroides* viability. The cellular requirement for MreB, and also the morphological defects associated with MreB loss, varies among bacterial species. In *E. coli* MreB is nonessential, as deletion of the gene produces a rounded morphology (12). In contrast, MreB appears essential for *B. subtilis* and *Caulobacter crescentus* viability, as MreB depletion produces abnormal morphologies and these aberrant cells eventually lyse (1, 7, 11). Given the more coccoid shape of photoheterotrophically grown *R. sphaeroides*, it seemed possible that these cells might not require MreB. Photoheterotrophic cells also show extensive invaginations of the cytoplasmic membrane and so might be unable to maintain a subcellular MreB structure. *mreB* deletion studies were attempted in *R. sphaeroides* grown aerobically or photoheterotrophically.

Attempts at mutating *R. sphaeroides mreB* by both in-frame deletion and insertional inactivation, under either aerobic or photoheterotrophic growth conditions, proved unsuccessful. These strategies have been routinely used to mutate nonessential genes in this bacterium (16), suggesting that MreB is essential in *R. sphaeroides* under both aerobic and photoheterotrophic growth conditions.

MreB depletion analysis in *R. sphaeroides* or creation of an *mreB* merodiploid strain was not possible due to the lack of an inducible expression system in this bacterium.

MreB localization in aerobic and photoheterotrophic cells. MreB localization varies among bacterial species. In *E. coli* MreB localizes in a helical configuration that spans the longitudinal axis of the cell and as a transverse band at mid-cell (20). In *B. subtilis* MreB localizes in a helical configuration mainly at mid-cell (11). As the cell shape and cytoplasmic membrane structure of *R. sphaeroides* changes under different growth conditions, immunofluorescence studies were carried out on *R. sphaeroides* cells grown aerobically and photoheterotrophically to determine MreB localization under conditions where the cell shape and the structure of the cytoplasmic membrane change.

In aerobically grown cells MreB localized predominantly as a transverse band or as opposing foci (Fig. 2A, row a). In addition patterns suggestive of a helical configuration, consisting of a transverse band and an adjacent focus, were observed in some cells (Fig. 2A, row a). In newly formed cells, opposing foci and transverse bands were observed slanting across the cell (Fig. 2A, set I in row b). In elongating cells transverse bands were observed at mid-cell (Fig. 2A, set II in row b). In cells beginning septation, opposing foci were observed at the site of septation (Fig. 2A, set III in row b). The localization at mid-cell appeared to break down before the completion of septation (Fig. 2A, set IV in row b), the localization at mid-cell being lost and reforming at mid-cell of the daughter cell. The localization pattern observed in *R. sphaeroides* suggests that MreB undergoes dynamic subcellular rearrangements during the cell cycle and that the protein may function at mid-cell with a possible role in early septation.

MreB immunofluorescence images of *R. sphaeroides* cells grown photoheterotrophically were similar to those of aerobic cells (Fig. 2B, row a). In newly formed cells, MreB was observed to be slanted at an angle across the cell width (Fig. 2B, set I in row b), and in elongating cells opposing foci were observed at mid-cell (Fig. 2B, set II in row b). The fluorescence remained associated with the septation site as division proceeded towards completion (Fig. 2B, sets III and IV in row b). The similar patterns of fluorescence observed in both aerobic and photoheterotrophic cells suggest that MreB performs a similar role under both growth conditions. While MreB may play a role in the regulation of cell shape, its localization to mid-cell in cells of varied lengths suggests it does not define cell length in *R. sphaeroides*.

MreB localization was similar in *R. sphaeroides* cells grown photoheterotrophically under either high or low light intensities. At low light intensities the cytoplasmic membrane of *R. sphaeroides* invaginates extensively to maximize the light-capturing and photosynthetic capacity of the photosynthesis apparatus (2). The MreB localization in cells grown under low light intensities (Fig. 2C) was similar to that found in both photoheterotrophic cells grown under much higher light intensities
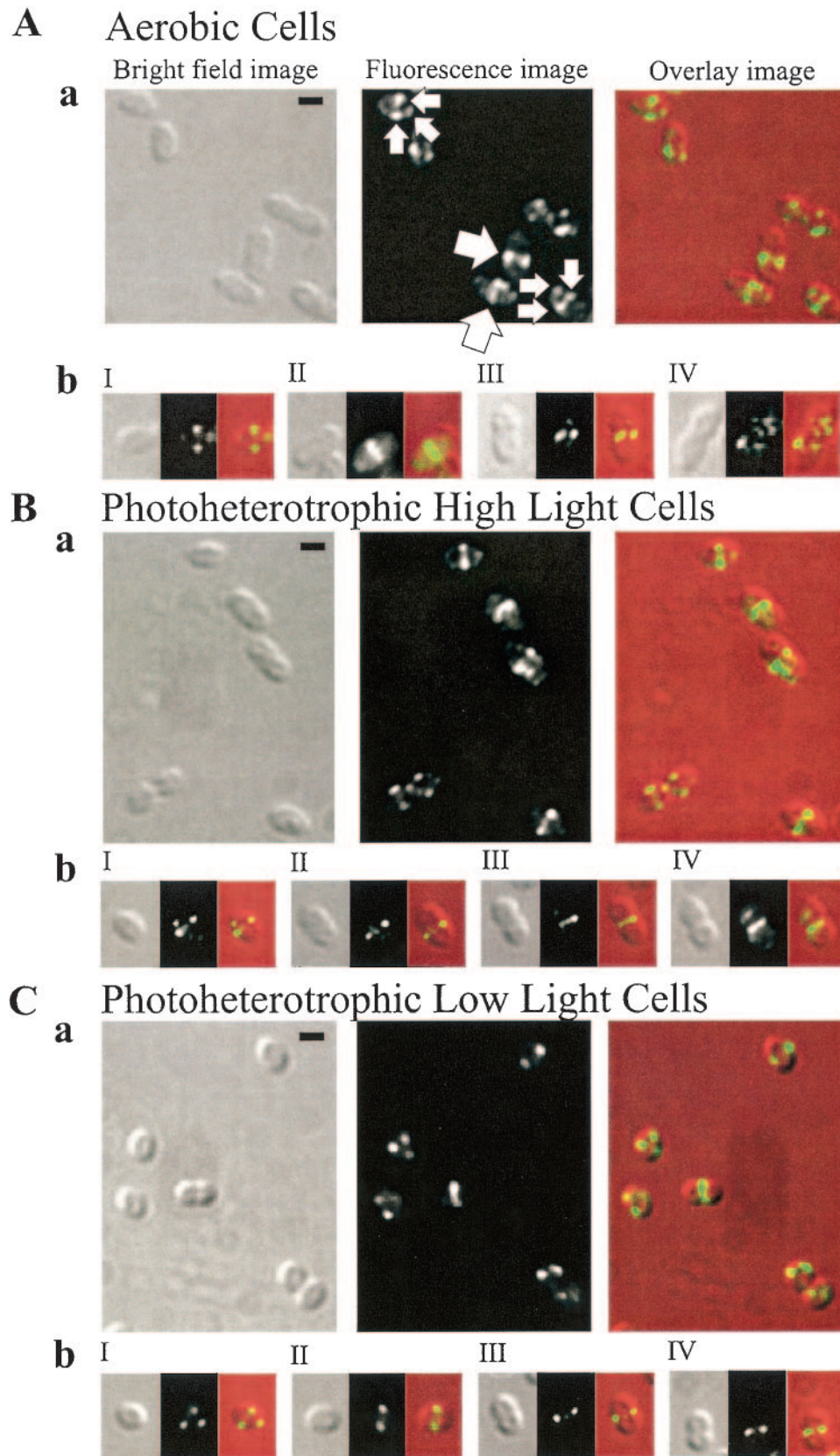
FIG. 2. Immunofluorescence localization of MreB in *R. sphaeroides*. (A) Localization in aerobic cells. (B) Localization in photoheterotrophic cells grown under high light. (C) Localization in photoheterotrophic cells grown under low light. Bright-field images, fluorescence images of the same field of cells, and an overlay of these images are shown (in that order). Large white arrows highlight transverse bands; small white arrows

and aerobic cells. The similar pattern of fluorescence suggests MreB performs the same role under these different growth conditions and again suggests that MreB does not form a subcellular structure defining *R. sphaeroides* cell length. Furthermore, MreB localization appears to be independent of the extensive cytoplasmic membrane rearrangements and consequent reorganization of the cytoplasm that occurs when cells are grown under low light conditions.

MreB forms a ring. Three-dimensional (3D) reconstructions of MreB in both *E. coli* and *B. subtilis* showed that the protein forms a helix in these bacteria (11, 20). 2D immunofluorescence localization of MreB in *R. sphaeroides* suggested that the protein forms a ring and/or a possible helix and, therefore, 3D reconstruction was carried out to establish which structure was formed.

3D reconstructions showed that the MreB subcellular structure was a ring (Fig. 3A). Images of an aerobic cell, including an MreB transverse band, were acquired (Fig. 3A, row a), and subsequently a z-series was captured. Deconvolution of these fluorescent images revealed a single focus at both the beginning and end of the z-series (Fig. 3A, row b) and two foci in the middle (Fig. 3A, row b). 3D reconstruction of the deconvolved z-series revealed an MreB ring (Fig. 3A, row c; see supplemental data).

Z-series acquisition, deconvolution, and 3D reconstruction were performed on an aerobic cell showing a possible helical MreB configuration in 2D images (Fig. 3B, row a). Deconvolution revealed that two of the three foci were the principle sources of fluorescence, and a similar pattern to that described above was found (Fig. 3B, row b). 3D reconstruction (Fig. 3B, row c; see supplemental data) showed that the helix-like configurations observed in some 2D images actually represented a slanted ring (Fig. 3B, row c, 90°) and a disconnected focus (Fig. 3B, row c, 0 and 180°).

MreB localization in filamentous cells. The antibiotic cephalexin inhibits FtsI, the septum-specific transpeptidase, resulting in the formation of filaments as the cells are unable to divide. In filamentous cells septation complexes based upon the essential septation protein FtsZ form at mid-cell and at other putative septation sites. Localization to these septation sites has previously been used to suggest protein involvement in septation.

In filamentous *R. sphaeroides* cells, MreB localized to both mid-cell and putative septation sites (Fig. 4). Transverse bands were observed at mid-cell (Fig. 4) with apparent helical configurations but, as above, probably represented a slanted ring and a disconnected focus (Fig. 4A) and transverse bands (Fig. 4B) also seen alongside this mid-cell localization. The localization to mid-cell and putative septation sites presumably reflect the assembly of septation complexes prior to, and following, the addition of cephalexin, respectively. This suggests that MreB in *R. sphaeroides* may be part of the septation complex.
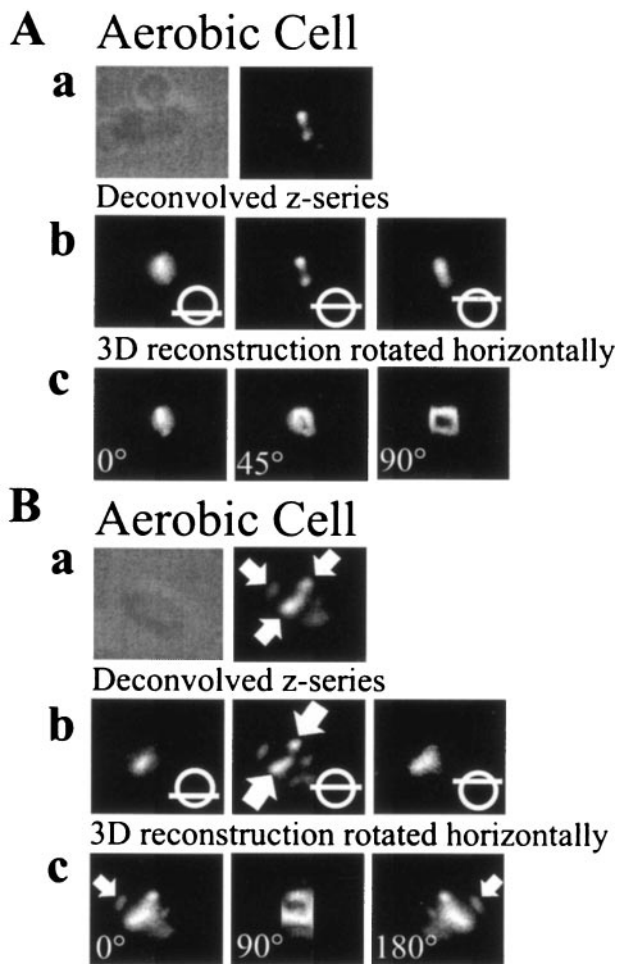
FIG. 3. 3D reconstruction of the MreB subcellular structure in *R. sphaeroides*. (A) Cell showing a transverse band of MreB in 2D. (B) Cell showing a helical configuration of MreB in 2D. (a) Bright-field and fluorescence images of aerobic cells. (b) Optical sections through these aerobic cells; the bottom, middle, and top of the z-series are shown. (c) 3D reconstruction of the z-series at 0, 45, and 90° for panel A and at 0, 90, and 180° for panel B. The images have been rotated horizontally. Small white arrows highlight the helix-like fluorescence; large white arrows highlight the principal sources of fluorescence. MreB forms a ring, not a helix, in *R. sphaeroides*.

GFP-MreB cell populations contain both normal- and abnormal-shaped cells. *R. sphaeroides* genomic *mreB* was replaced with a *gfp-mreB* fusion. The N-terminal fusion was constructed and inserted into the genome as described previously (32) to create *R. sphaeroides* strain JPA187. This strategy ensured that a single copy of *gfp-mreB* was expressed from its native promoter in the *R. sphaeroides* genome. The growth rate was determined for wild-type and GFP-MreB-expressing cells: wild-type cells had a doubling time of 170 min, while GFP-MreB

highlight helix-like configurations. (a) Representative field of cells; (b) cells representing the different stages of the cell cycle: newly formed (I), elongating (II), septation initiated (III), and septation nearing completion (IV). MreB localizes predominantly as a transverse band. In newly formed cells, MreB slants across the cell close to the cell periphery. In elongating cells, MreB forms a transverse band at mid-cell. MreB remains at mid-cell or at the septation site in cells beginning septation. This localization pattern is observed in cells grown aerobically and photoheterotrophically. Bars, 1 μm.
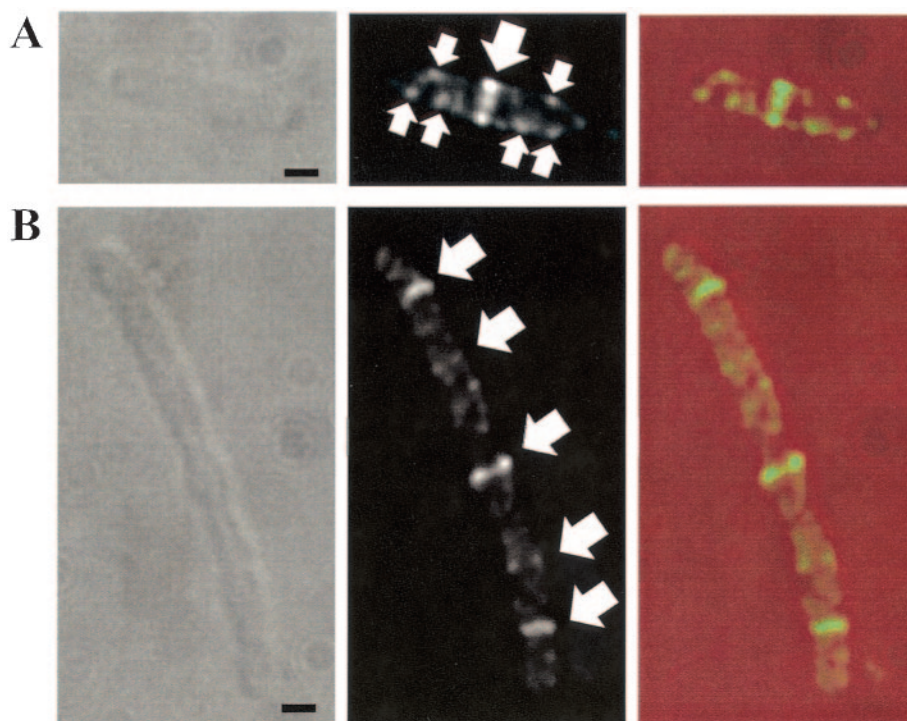
FIG. 4. Immunofluorescence localization of MreB in *R. sphaeroides* treated with cephalexin. (A) Short filament; (B) long filament. Bright-field images, fluorescence images of the same filament, and an overlay of these images are shown (in that order). MreB localized as a transverse band (large white arrows) at the mid-cell septation site. Helical configurations (small white arrows) and transverse bands (large white arrows) were also observed alongside this mid-cell localization. Bar, 1 μm.

cells had a doubling time of 247 min (data not shown). This suggests that the GFP-MreB fusion is only partially functional.

Populations of GFP-MreB-expressing cells contained both normal- and abnormal-shaped cells (Fig. 5). Normal-shaped cells showed at worst a modest increase in cell width (≤9%) in comparison to wild type. These cells accounted for 49% of the population. Abnormal-shaped cells varied in their degree of abnormality. In mildly abnormal cells, the cell width increased (≥20%) in comparison to wild type. In severely abnormal cells, both the cell width (≥33%) and cell length (≥23%) increased in comparison to wild type. These changes were observed at all stages of the cell cycle. A few severely abnormal cells showed a decrease in cell length (≥12%) in comparison to wild type (data not shown). The peptidoglycan layer ultimately governs the cell shape of bacteria. Thus, the abnormal morphologies in GFP-MreB-expressing populations suggest that MreB may be involved in the cytoplasmic control of peptidoglycan synthesis.

MreB localization in normal cells confirmed the immunofluorescence results (Fig. 6). GFP-MreB was slanted across the cell close to the cell periphery in newly formed cells (Fig. 6A), and in elongating cells GFP-MreB formed a transverse band at mid-cell (Fig. 6A). Localization of MreB was followed through the cell cycle (Fig. 6B). In cells undergoing septation, GFP-MreB localized to the septation site as a transverse band close to the leading edge of cellular constriction (Fig. 6B, set I). As found in the immunofluorescence studies, the MreB structure appeared to break down before the completion of septation (Fig. 6B, set II). GFP-MreB was slanted across the newly formed cell (Fig. 6B, sets III and V) and formed a transverse band at mid-cell as elongation proceeded (Fig. 6B, sets VI to

VIII). GFP-MreB again localized to the septation site as septation ensued (Fig. 6B, sets IX and X). As with the immunofluorescence data, the localization of GFP-MreB suggests that the MreB structure undergoes dynamic rearrangements during the cell cycle and that the protein may function at mid-cell, potentially including a role in early septation.

MreB localization in amdinocillin-treated cells. Penicillin antibiotics cause bacteria to swell at the future or current site of septation. Amdinocillin, which specifically inhibits PBP2-mediated elongation of the side wall, was added to GFP-MreB populations to cause swelling at these sites and identify whether these regions related to sites of GFP-MreB localization.

Wild-type and GFP-MreB cells bulged at mid-cell in the presence of amdinocillin (Fig. 7). GFP-MreB was observed at these swollen sites as transverse bands or opposing foci close to the cell periphery. The maintenance of GFP-MreB localization in cells with aberrant morphologies again suggests that the MreB subcellular structure does not define *R. sphaeroides* morphology but may have a role in septation or peptidoglycan insertion.

DISCUSSION

The *R. sphaeroides* WS8N *mre* and *mrd* genetic loci form a putative operon. In *E. coli* the *mre* locus forms an operon with two genes of unknown function (30), while the *mrd* locus is located elsewhere on the genome (25). In *B. subtilis* the *mre* locus forms an operon with *minC* and *minD* (13), whose protein products function in the correct placement of the FtsZ ring (20). The genetic arrangement observed in *R. sphaeroides*

Cell cycle stage and cell shape properties	*R. sphaeroides* genotype and phenotype			
	Wild-type	GFP-MreB expressing cells		
		'Normal'	'Mildly abnormal'	'Severely abnormal'
Newly formed				
Length (μm, ±SE)	1.74±0.02	1.73±0.02	1.75±0.05	2.34±0.15
Width (μm, ±SE)	1.16±0.01	1.27±0.01	1.40±0.03	1.64±0.07
Elongating				
Length (μm, ±SE)	2.22±0.03	2.12±0.03	2.23±0.04	2.72±0.08
Width (μm, ±SE)	1.17±0.01	1.26±0.01	1.48±0.02	1.59±0.03
Septation initiated				
Length (μm, ±SE)	2.62±0.02	2.63±0.02	2.76±0.05	3.33±0.10
Width (μm, ±SE)	1.17±0.01	1.25±0.01	1.40±0.02	1.56±0.03
Septation nearing completion				
Length (μm, ±SE)	2.99±0.03	2.93±0.02	3.20±0.06	4.00±0.15
Width (μm, ±SE)	1.17±0.01	1.28±0.01	1.47±0.03	1.63±0.03
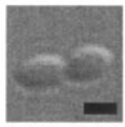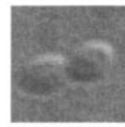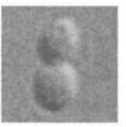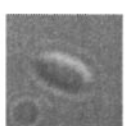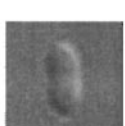
FIG. 5. Cell shape properties of *R. sphaeroides* populations expressing GFP-MreB. Representational images, cell lengths, and cell widths are shown of aerobically grown wild-type and GFP-MreB-expressing cells. Populations of GFP-MreB-expressing cells were divided into normal, mildly abnormal, and severely abnormal categories. For the wild-type cells, a total of ≥25 cells were analyzed, from ≥5 fields of view, for each cell cycle stage. For GFP-MreB-expressing populations, a total of ≥25 normal, mildly abnormal, or severely abnormal cells were analyzed, from ≥10 fields of view, for each cell cycle stage. Mean values and standard errors are shown. Normal cells expressing GFP-MreB resembled wild-type cells throughout the cell cycle. Mildly abnormal cells displayed a ≥20% increase in cell width. Severely abnormal cells displayed a ≥23% increase in cell length and a ≥33% increase in cell width. Bar, 1 μm. All images are to the same scale.

is also found in *Streptomyces coelicolor* and in *C. crescentus* (1, 7) and suggests a functional interaction exists between the protein products.

The requirement for MreB varies among bacterial species. In *E. coli mreB* deletion produces spherical bacteria (12), whereas in *S. coelicolor* the gene cannot be deleted (1) and in *B. subtilis* and in *C. crescentus* MreB depletion causes cells to swell and lyse (7, 11). *R. sphaeroides* MreB also appears to be essential, as we were unable to delete or insertionally inactivate *mreB* using techniques standard for this species. This was supported by the abnormal cell shapes observed in some cells in which *mreB* was replaced with *gfp-mreB* and the reduced growth rate of this strain. The different requirement for MreB between the gram-negative *E. coli* and gram-positive *B. subtilis* and *S. coelicolor* had been attributed to differences in the cellular envelopes of these species. However, as MreB also appears to be essential in the gram-negative *R. sphaeroides* and

C. crescentus, the underlying principle governing MreB requirement in bacteria is therefore uncertain.

R. sphaeroides MreB localized predominantly as a transverse band at mid-cell, and 3D reconstruction showed that it formed a ring. 2D immunofluorescence images also showed foci in some cells that could reflect a helical structure, but 3D reconstruction showed that these foci represented a slanted ring and disconnected foci rather than a helix. The disconnected foci may represent past or future sites of MreB localization; the protein may be in transit to its mid-cell destination. The localization and subcellular structure of MreB appears to vary between bacterial species. In *E. coli* and *C. crescentus* MreB localizes in both a helical configuration that spans the longitudinal axis of the cell and as a transverse band at mid-cell (7, 20). In *B. subtilis* MreB localizes as a helix, mainly at mid-cell (11). The mid-cell MreB localization is conserved among both gram-negative and gram-positive bacteria, suggesting that, al-
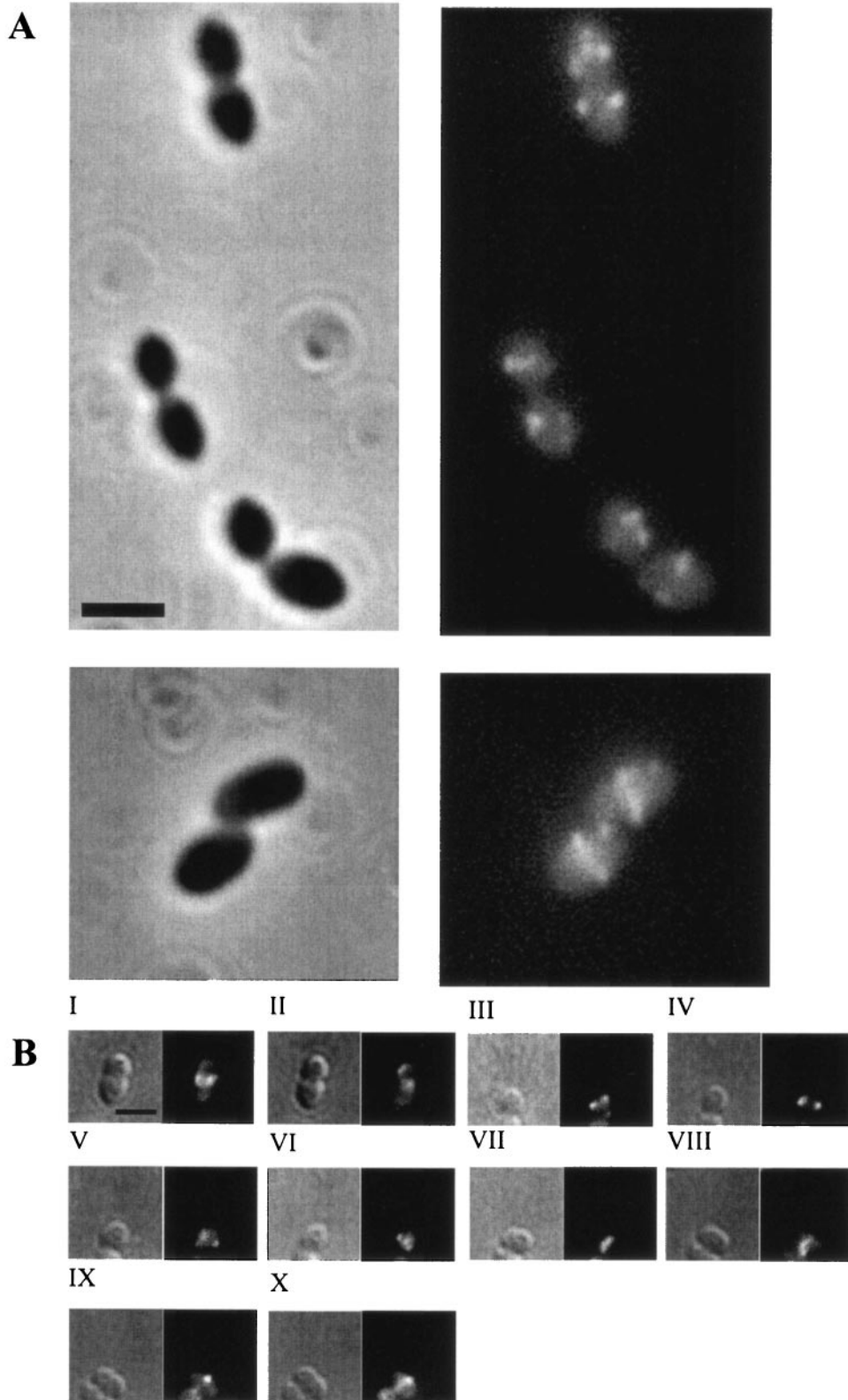
FIG. 6. Localization of GFP-MreB in normal cells. Bright-field images are shown on the left, and their corresponding fluorescence images are on the right. (A) Localization in normal cells expressing GFP-MreB. (B) Localization in a normal cell throughout the cell cycle; images (I to X) were acquired at 20-min intervals. Note, the cell shown has rotated on the slide during growth and division, accounting for the variation in orientation of the MreB fluorescence. The GFP-MreB localization confirmed the immunofluorescence microscopy results. Bars, 2 μm.
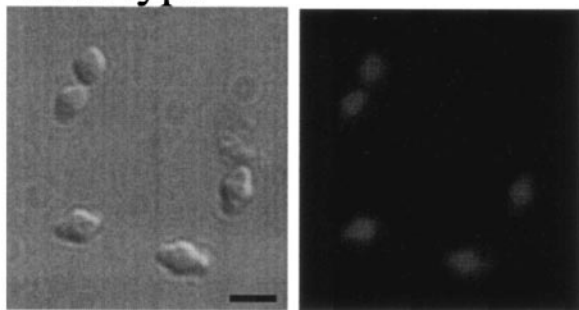
A Wild-type

B GFP-MreB expressing
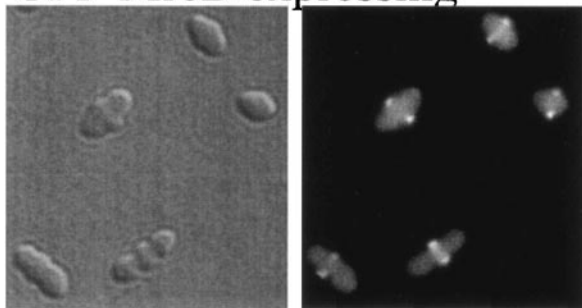
FIG. 7. *R. sphaeroides* cells treated with amdinocillin, an inhibitor of PBP2. Bright-field images are shown on the left, and their corresponding fluorescence images are on the right. (A) Wild-type cells following amdinocillin treatment. (B) GFP-MreB-expressing cells following amdinocillin treatment. GFP-MreB localized as transverse bands at swellings at mid-cell. Bar, 2 μm.

though the subcellular structure may vary, MreB performs a similar role at this site in all bacteria possessing this protein.

R. sphaeroides MreB localization appears characteristic of a septation protein. MreB localized at mid-cell in elongating cells and remained at this site, i.e., the site of septation, as septation began. Furthermore, the protein formed a ring at mid-cell, and the localization pattern in filamentous cells was characteristic of septation proteins. MreB localization at mid-cell has also been observed in *E. coli*, *B. subtilis*, and *C. crescentus* (7, 11, 20); furthermore, in *C. crescentus* this localization depends upon the tubulin homolog FtsZ (6, 7). Early in the cell cycle, FtsZ localizes to mid-cell and forms a ring at the future site of septation termed the Z-ring. Proteins of the division complex assemble in a specific sequence to the Z-ring, forming the so-called divisome, which is capable of cytokinesis. MreB may therefore be part of the divisome. The putative role for the bacterial actin homolog MreB at the site of septation extends the functional relationship between prokaryotic MreB and eukaryotic actin by including a shared role in cytokinesis in their respective kingdoms.

In *R. sphaeroides* the *mre* locus was found to overlap with the *mrd* locus, and the partially functional GFP-MreB fusion resulted in abnormalities in cell shape. Thus, in *R. sphaeroides*, MreB may function in the cytoplasmic control of the peptidoglycan-synthetic complexes that ultimately govern cell shape. In *E. coli mreB* deletion produces spherical cells, i.e., there is no extension of the longitudinal axis (12), and *mre* mutations are associated with altered sensitivities to the PBP2-specific

amdinocillin (29). In *B. subtilis* and in *C. crescentus* MreB depletion produces abnormal cell shapes (11) similar to the morphologies created by PBP inhibition (4), and in *C. crescentus* PBP2 localization is dependent upon MreB (7). The accumulated experimental data suggest that MreB plays a role in the cytoplasmic control of the synthetic complexes that form the peptidoglycan layer, which ultimately governs cell shape.

In *B. subtilis* the MreB localization and depletion studies led to the proposal that the protein also forms a subcellular structure that also helps define the rod cell shape (11). In *R. sphaeroides* MreB localization was similar in both long aerobic cells and comparatively short photoheterotrophic cells and was predominantly localized at mid-cell. These data, combined with the potentially essential nature of the gene and the abnormal cellular morphologies seen in some cells expressing a GFP-MreB fusion, suggest MreB may function at mid-cell to regulate the synthesis and deposition of peptidoglycan, governing cell shape by controlling synthesis of the cell wall rather than by forming a static subcellular structure defining rod-shaped cells. Furthermore, the similar localization in both aerobic and photoheterotrophic cells, possessing different patterns of membrane invagination, suggests that the cytoplasmic membrane must be demarcated with specific regions prevented from forming invaginations to allow for housekeeping cellular functions.

The precise role of MreB remains uncertain. In *R. sphaeroides*, the experimental data are suggestive of an involvement in both early septation and peptidoglycan synthesis. The result associating MreB with peptidoglycan formation, i.e., the abnormal shapes in some cells expressing GFP-MreB, suggests that the principle function of MreB is at sites of peptidoglycan insertion. Consequently, the localization at mid-cell may reflect the fact that this region is the main site of peptidoglycan synthesis rather than suggesting a specific role for MreB in septation.

REFERENCES

1. **Burger, A., K. Sichler, G. Kelemen, M. Buttner, and W. Wohlleben.** 2000. Identification and characterization of the *mre* gene region of *Streptomyces coelicolor* A3(2). Mol. Gen. Genet. **263:**1053–1060.
2. **Chory, J., T. J. Donohue, A. R. Varga, L. A. Staehelin, and S. Kaplan.** 1984. Induction of the photosynthetic membranes of *Rhodopseudomonas sphaeroides*: biochemical and morphological studies. J. Bacteriol. **159:**540–554.
3. **De Pedro, M. A., W. D. Donachie, J. V. Holtje, and H. Schwarz.** 2001. Constitutive septal murein synthesis in *Escherichia coli* with impaired activity of the morphogenetic proteins RodA and penicillin-binding protein 2. J. Bacteriol. **183:**4115–4126.
4. **De Pedro, M. A., H. Schwarz, and A. L. Koch.** 2003. Patchiness of murein insertion into the sidewall of *Escherichia coli*. Microbiology **149:**1753–1761.
5. **Erickson, H. P.** 2001. Evolution in bacteria. Nature **413:**30.
6. **Errington, J., R. A. Daniel, and D. J. Scheffers.** 2003. Cytokinesis in bacteria. Microbiol. Mol. Biol. Rev. **67:**52–65.
7. **Figge, R. M., A. V. Divakaruni, and J. W. Gober.** 2004. MreB, the cell shape-determining bacterial actin homologue, co-ordinates cell wall morphogenesis in *Caulobacter crescentus*. Mol. Microbiol. **51:**1321–1332.
8. **Hamblin, P. A., N. A. Bourne, and J. P. Armitage.** 1997. Characterization of the chemotaxis protein CheW from *Rhodobacter sphaeroides* and its effect on the behaviour of *Escherichia coli*. Mol. Microbiol. **24:**41–51.
9. **Harry, E. J., K. Pogliano, and R. Losick.** 1995. Use of immunofluorescence to visualize cell-specific gene expression during sporulation in *Bacillus subtilis*. J. Bacteriol. **177:**3386–3393.
10. **Hofmann, K., and W. Stoffel.** 1993. TMbase: a database of membrane spanning protein segments. Biol. Chem. Hoppe-Seyler **374:**166.

11. **Jones, L. J. F., R. Carballido-Lopez, and J. Errington.** 2001. Control of cell shape in bacteria: helical, actin-like filaments in *Bacillus subtilis*. Cell **104:** 913–922.

12. **Kruse, T., J. Moller-Jensen, A. Lobner-Olesen, and K. Gerdes.** 2003. Dysfunctional MreB inhibits chromosome segregation in *Escherichia coli*. EMBO J. **22:** 5283–5292.

13. **Levin, P. A., P. S. Margolis, P. Setlow, R. Losick, and D. X. Sun.** 1992. Identification of *Bacillus subtilis* genes for septum placement and shape determination. J. Bacteriol. **174:** 6717–6728.

14. **Martin, A. C., G. H. Wadhams, D. S. H. Shah, S. L. Porter, J. C. Mantotta, T. J. Craig, P. H. Verdult, H. Jones, and J. P. Armitage.** 2001. CheR- and CheB-dependent chemosensory adaptation system of *Rhodobacter sphaeroides*. J. Bacteriol. **183:** 7135–7144.

15. **Penfold, R. J., and J. M. Pemberton.** 1992. An improved suicide vector for construction of chromosomal insertion mutations in bacteria. Gene **118:** 145–146.

16. **Porter, S. L., A. V. Warren, A. C. Martin, and J. P. Armitage.** 2002. The third chemotaxis locus of *Rhodobacter sphaeroides* is essential for chemotaxis. Mol. Microbiol. **46:** 1081–1094.

17. **Prentki, P., and H. M. Krisch.** 1984. *In vitro* insertional mutagenesis with a selectable DNA fragment. Gene **29:** 303–313.

18. **Sambrook, J., and D. W. Russell.** 2001. Molecular cloning: a laboratory manual, 3rd ed. Cold Spring Harbor Laboratory Press, Cold Spring Harbor, N.Y.

19. **Schäfer, A., A. Tauch, W. Jager, J. Kalinowski, G. Thierbach, and A. Puhler.** 1994. Small mobilizable multipurpose cloning vectors derived from the *Escherichia coli* plasmids pK18 and pK19: selection of defined deletions in the chromosome of *Corynebacterium glutamicum*. Gene **145:** 69–73.

20. **Shih, Y. L., T. Le, and L. Rothfield.** 2003. Division site selection in *Escherichia coli* involves dynamic redistribution of Min proteins within coiled structures that extend between the two cell poles. Proc. Natl. Acad. Sci. USA **100:** 7865–7870.

21. **Sistrom, W. R.** 1960. A requirement for sodium in the growth of *Rhodopseudomonas sphaeroides*. J. Gen. Appl. Microbiol. **22:** 778–785.

22. **Sockett, R. E., and J. P. Armitage.** 1991. Isolation, characterization, and complementation of a paralyzed flagellar mutant of *Rhodobacter sphaeroides* WS8. J. Bacteriol. **173:** 2786–2790.

23. **Sockett, R. E., J. C. A. Foster, and J. P. Armitage.** 1990. Molecular biology of the *Rhodobacter sphaeroides* flagellum. FEMS Symp. **53:** 473–479.

24. **Soufo, H. J. D., and P. L. Graumann.** 2003. Actin-like proteins MreB and Mbl from *Bacillus subtilis* are required for bipolar positioning of replication origins. Curr. Biol. **13:** 1916–1920.

25. **Tamaki, S., H. Matsuzawa, and M. Matsuhashi.** 1980. Cluster of *mrdA* and *mrdB* genes responsible for the rod shape and mecillinam sensitivity of *Escherichia coli*. J. Bacteriol. **141:** 52–57.

26. **van den Ent, F., L. A. Amos, and J. Lowe.** 2001. Prokaryotic origin of the actin cytoskeleton. Nature **413:** 39–44.

27. **Varley, A. W., and G. C. Stewart.** 1992. The *divIVB* region of the *Bacillus subtilis* chromosome encodes homologs of *Escherichia coli* septum placement (MinCD) and cell shape (MreBCD) determinants. J. Bacteriol. **174:** 6729–6742.

28. **Wachi, M., M. Doi, Y. Okada, and M. Matsuhashi.** 1989. New *mre* genes *mreC* and *mreD*, responsible for formation of the rod shape of *Escherichia coli* cells. J. Bacteriol. **171:** 6511–6516.

29. **Wachi, M., M. Doi, S. Tamaki, W. Park, S. Nakajimaiijima, and M. Matsuhashi.** 1987. Mutant isolation and molecular cloning of *mre* genes, which determine cell shape, sensitivity to mecillinam, and amount of penicillin-binding proteins in *Escherichia coli*. J. Bacteriol. **169:** 4935–4940.

30. **Wachi, M., M. Doi, T. Ueda, M. Ueki, K. Tsuritani, K. Nagai, and M. Matsuhashi.** 1991. Sequence of the downstream flanking region of the shape-determining genes *mreBCD* of *Escherichia coli*. Gene **106:** 135–136.

31. **Wadhams, G. H., A. C. Martin, and J. P. Armitage.** 2000. Identification and localization of a methyl-accepting chemotaxis protein in *Rhodobacter sphaeroides*. Mol. Microbiol. **36:** 1222–1233.

32. **Wadhams, G. H., A. V. Warren, A. C. Martin, and J. P. Armitage.** 2003. Targeting of two signal transduction pathways to different regions of the bacterial cell. Mol. Microbiol. **50:** 763–770.